ELSEVIER

Probabilistic Engineering Mechanics 20 (2005) 239–250

PROBABILISTIC ENGINEERING MECHANICS

www.elsevier.com/locate/probengmech

Decomposition methods for structural reliability analysis

H. Xu, S. Rahman*

Department of Mechanical Engineering, The University of Iowa, 2140 Seamans Center, Iowa City, IA 52242, USA

Available online 19 July 2005

Abstract

A new class of computational methods, referred to as decomposition methods, has been developed for predicting failure probability of structural and mechanical systems subject to random loads, material properties, and geometry. The methods involve a novel function decomposition that facilitates univariate and bivariate approximations of a general multivariate function, response surface generation of univariate and bivariate functions, and Monte Carlo simulation. Due to a small number of original function evaluations, the proposed methods are very effective, particularly when a response evaluation entails costly finite-element, mesh-free, or other numerical analysis. Seven numerical examples involving elementary mathematical functions and solid-mechanics problems illustrate the methods developed. Results indicate that the proposed methods provide accurate and computationally efficient estimates of probability of failure.

Keywords: Reliability; Decomposition; Univariate method; Bivariate method; Response surface; Stochastic finite-element and mesh-free methods

1. Introduction

A fundamental problem in the time-invariant reliability analysis entails calculation of a multi-fold integral [1–3]

$$P_{\mathrm{F}} \equiv P(\boldsymbol{X} \in \Omega_{\mathrm{F}}) = \int_{\Omega_{\mathrm{F}}} f_X(\boldsymbol{x})\mathrm{d}\boldsymbol{x}, \tag{1}$$

where $\boldsymbol{X} = \{X_1, \ldots, X_N\}^{\mathrm{T}} \in \mathbb{R}^N$ is a real-valued, N-dimensional random vector defined on a probability space (Ω, $\mathcal{F}$, P) comprising the sample space Ω, the σ-field $\mathcal{F}$, and the probability measure P; Ω_{F} is the failure domain; and $f_X(\boldsymbol{x})$ is the joint probability density function of $\boldsymbol{X}$. In structural reliability analysis, $\boldsymbol{X}$ typically represents loads, material properties, and geometry and P_{F} is the probability of failure. For component reliability analysis, $\Omega_{\mathrm{F}} = \{\boldsymbol{x}: y(\boldsymbol{x}) < 0\}$, where $y(\boldsymbol{x})$ represents a single performance function. For system reliability analyses involving m performance functions, $\Omega_{\mathrm{F}} = \{\boldsymbol{x} : \cup_{k=1}^{m} y^{(k)}(\boldsymbol{x}) < 0\}$ and $\Omega_{\mathrm{F}} = \{\boldsymbol{x} : \cap_{k=1}^{m} y^{(k)}(\boldsymbol{x}) < 0\}$ for series and parallel systems, respectively, where $y^{(k)}(\boldsymbol{x})$ represents the kth performance function. Nevertheless, for most practical problems, the exact evaluation of this integral, either analytically or numerically, is not possible because N is large, $f_{\boldsymbol{x}}(\boldsymbol{x})$ is generally non-Gaussian, and $y(\boldsymbol{x})$ or $y^{(k)}(\boldsymbol{x})$ are highly nonlinear functions of $\boldsymbol{x}$. While research is ongoing, approximate methods, such as the first- and second-order reliability methods (FORM/SORM) [1–8] and simulation methods [9–18] are commonly employed to estimate the failure probability.

FORM/SORM are based on linear (FORM) or quadratic approximation (SORM) of the limit-state surface at a most probable point (MPP). Experience has shown that FORM/SORM are sufficiently accurate for engineering purposes, provided that the MPP is accurately found, the limit-state surface at MPP is close to being linear or quadratic, and no multiple MPPs exist. The MPP can be located by various gradient-based optimization algorithms, which in turn require first- and/or second-order (also needed in SORM) response sensitivities or gradients, for which efficient means of calculation are also required. If these sensitivities can be calculated analytically, FORM/SORM are quite efficient. Otherwise, FORM/SORM can be ineffective, for instance, when response sensitivities are not available or when sensitivity analysis is computationally intensive. A prime example is a multidisciplinary design environment, where multiple analysis codes from third-party sources are frequently employed without any knowledge of gradients. In that case, FORM/SORM may yield inaccurate reliability solutions

* Corresponding author. Tel.: +1 319 335 5679; fax: +1 319 335 5669.
E-mail address: rahman@engineering.uiowa.edu (S. Rahman).
URL: http://www.engineering.uiowa.edu/~rahman.

0266-8920/$ - see front matter © 2005 Elsevier Ltd. All rights reserved.
doi:10.1016/j.probengmech.2005.05.005

or create computationally inefficient results when using gradients from finite-difference approximations. Furthermore, for highly nonlinear performance functions, which exist in many structural problems, results based on FORM/SORM must be interpreted with caution. If the Rosenblatt transformation, frequently used to map non-Gaussian random input into its standard Gaussian image, yields a highly nonlinear limit-state, inadequate reliability estimates by FORM/SORM may result [12,13]. Furthermore, the existence of multiple MPPs could give rise to large errors in standard FORM/SORM approximations [3,8]. In that case, multi-point FORM/SORM along with the system reliability concept is required for improving component reliability analysis [8].

Simulation methods involving sampling and estimation are well known in the statistics and reliability literature. Direct Monte Carlo simulation [9] is the most widely used simulation method and involves the generation of independent samples of all input random variables, repeated deterministic trials (analyses) to obtain corresponding simulated samples of response variables, and standard statistical analysis to estimate probabilistic characteristics of response. This method generally requires a large number of simulations to calculate low failure probability, and is impractical when each simulation involves expensive finite-element, boundary-element, or mesh-free calculations. As a result, researchers have developed or examined faster simulation methods, such as quasi-Monte Carlo simulation [10], importance sampling [11], directional simulation [12–14], and others [15–18]. While simulation methods do not exhibit the limitations of approximate reliability methods, such as FORM/SORM, they generally require considerably more extensive calculations than the latter methods. Consequently, simulation methods are useful when alternative methods are inapplicable or inaccurate, and have been traditionally employed as a yardstick for evaluating approximate methods.

This paper presents a new class of computational methods, referred to as decomposition methods, for predicting reliability of structural and mechanical systems subject to random loads, material properties, and geometry. The idea of decomposition in multivariate functions, originally developed by the authors for statistical moment analysis [19,20], has been extended for reliability analysis, which is the focus of the current paper. The proposed reliability methods involve a very small number of exact or numerical evaluations of the performance function at selected input, generation of approximate values of the performance function at arbitrarily large number of input using the decomposition technique, and subsequent response surface approximations. Finally, the reliability is evaluated using the Monte Carlo simulation. Seven numerical examples involving elementary mathematical functions and solid-mechanics problems illustrate the proposed method. Whenever possible, comparisons have been made with alternative approximate and simulation methods to evaluate the accuracy and computational efficiency of the proposed methods.

2. Multivariate function decomposition

Consider a continuous, differentiable, real-valued function $y(\boldsymbol{x})$ that depends on $\boldsymbol{x}=\{x_1,\ldots,x_N\}^{\mathrm{T}}\in\mathbb{R}^N$. Suppose that $y(\boldsymbol{x})$ has a convergent Taylor series expansion at an arbitrary reference point $\boldsymbol{x}=\boldsymbol{c}=\{c_1,\ldots,c_N\}^{\mathrm{T}}$, expressed by

$$y(\boldsymbol{x}) = y(\boldsymbol{c}) + \sum_{j=1}^{\infty}\frac{1}{j!}\sum_{i=1}^{N}\frac{\partial^j y}{\partial x_i}(\boldsymbol{c})(x_i-c_i)^j + \mathcal{R}_2, \tag{2}$$

or

$$y(\boldsymbol{x}) = y(\boldsymbol{c}) + \sum_{j=1}^{\infty}\frac{1}{j!}\sum_{i=1}^{N}\frac{\partial^j y}{\partial x_i}(\boldsymbol{c})(x_i-c_i)^j + \sum_{j_1 j_2>0}^{\infty}\frac{1}{j_1!j_2!}\sum_{i_1<i_2}\frac{\partial^{j_1+j_2} y}{\partial x_{i_1}^{j_1}\partial x_{i_2}^{j_2}}(\boldsymbol{c})(x_{i_1}-c_{i_1})^{j_1}(x_{i_2}-c_{i_2})^{j_2} + \mathcal{R}_3, \tag{3}$$

where the remainder $\mathcal{R}_2$ denotes all terms with dimension two and higher and the remainder $\mathcal{R}_3$ denotes all terms with dimension three and higher.

2.1. Univariate approximation

Consider a univariate approximation of $y(\boldsymbol{x})$, denoted by

$$\hat{y}_1(\boldsymbol{x}) \equiv \hat{y}_1(x_1,\ldots,x_N) = \sum_{i=1}^{N} y(c_1,\ldots,c_{i-1},x_i,c_{i+1},\ldots,c_N) - (N-1)y(\boldsymbol{c}), \tag{4}$$

where each term in the summation is a function of only one variable and can be subsequently expanded in a Taylor series at $\boldsymbol{x}=\boldsymbol{c}$, yielding

$$\hat{y}_1(\boldsymbol{x}) = y(\boldsymbol{c}) + \sum_{j=1}^{\infty}\frac{1}{j!}\sum_{i=1}^{N}\frac{\partial^j y}{\partial x_i^j}(\boldsymbol{c})(x_i-c_i)^j. \tag{5}$$

Comparing Eqs. (2) and (5) indicates that the univariate approximation leads to the residual error $y(\boldsymbol{x})-\hat{y}_1(\boldsymbol{x})=\mathcal{R}_2$, which includes contributions from terms of dimension two and higher. For sufficiently smooth $y(\boldsymbol{x})$ with convergent Taylor series, the coefficients associated with higher-dimensional terms are usually much smaller than that with one-dimensional terms. In that case, higher-dimensional terms contribute less to the function, and therefore, can be neglected. Furthermore, Eq. (4) represents exactly the same function as $y(\boldsymbol{x})$ when $y(\boldsymbol{x})=\sum_i y_i(x_i)$, i.e. when $y(\boldsymbol{x})$ can be additively decomposed into functions $y_i(x_i)$ of single variables.

2.2. Bivariate approximation

In the similar way, consider a bivariate approximation

$$\begin{aligned}\hat{y}_2(\boldsymbol{x}) &\equiv \sum_{i_1<i_2} y(c_1,\ldots,c_{i_1-1},x_{i_1},c_{i_1+1},\ldots,c_{i_2-1},x_{i_2},c_{i_2+1},\ldots,c_N) \\ &\quad -(N-2)\sum_{i=1}^{N} y(c_1,\ldots,c_{i-1},x_i,c_{i+1},\ldots,c_N) \\ &\quad +\frac{(N-1)(N-2)}{2}y(\boldsymbol{c}),\end{aligned} \tag{6}$$

of $y(\boldsymbol{x})$, where each term on the right hand side is a function of at most two variables and can be subsequently expanded in a Taylor series at $\boldsymbol{x}=\boldsymbol{c}$, yielding

$$\begin{aligned}\hat{y}_2(\boldsymbol{x}) &= y(\boldsymbol{c}) + \sum_{j=1}^{\infty}\frac{1}{j!}\sum_{i=1}^{N}\frac{\partial^j y}{\partial x_i}(\boldsymbol{c})(x_i-c_i)^j \\ &\quad + \sum_{j_1,j_2>0}^{\infty}\frac{1}{j_1!j_2!}\sum_{i_1<i_2}\frac{\partial^{j_1+j_2}y}{\partial x_{i_1}\partial x_{i_2}}(\boldsymbol{c})(x_{i_1}-c_{i_1})^{j_1}(x_{i_2}-c_{i_2})^{j_2}.\end{aligned} \tag{7}$$

Again, the comparison of Eqs. (3) and (7) indicates that the bivariate approximation leads to the residual error $y(\boldsymbol{x})-\hat{y}_2(\boldsymbol{x})=\mathcal{R}_3$, in which remainder $\mathcal{R}_3$ includes terms of dimension three and higher. The bivariate approximation includes all terms with no more than two variables, thus leads to higher accuracy than the univariate approximation. Furthermore, Eq. (6) represents exactly the same function as $y(\boldsymbol{x})$ when $y(\boldsymbol{x})=\sum_{i<j}y_{ij}(x_i,x_j)$, i.e. when $y(\boldsymbol{x})$ can be additively decomposed into functions $y_{ij}(x_i, x_j)$ of at most two variables.

2.3. Generalized S-variate approximation

The procedure for univariate and bivariate approximations described in the preceding can be generalized to an S-variate approximation for any integer $1\le S\le N$. The generalized S-variate approximation of $y(\boldsymbol{x})$ is

$$\begin{aligned}\hat{y}_S(\boldsymbol{x}) &\equiv \sum_{i=0}^{S}(-1)^i\binom{N-S+i-1}{i} \\ &\quad \times \sum_{k_1<\cdots<k_{S-i}} y(c_1,\ldots,c_{k_1-1},x_{k_1},c_{k_1+1},\ldots,c_{k_{S-i}-1},x_{k_{S-i}}, \\ &\quad c_{k_{S-i}+1},\ldots,c_N).\end{aligned} \tag{8}$$

If $y_R\equiv y(c_1,\ldots,c_{k_1-1},x_{k_1},c_{k_1+1},\ldots,c_{k_R-1},x_{k_R},c_{k_R+1},\ldots,c_N)$; $0\le R\le S$, a multivariate function decomposition theorem developed by the authors leads to [20]

$$y_R=\sum_{k=0}^{R}\binom{N-k}{R-k}t_k;\qquad 0\le R\le S, \tag{9}$$

where

$$\begin{aligned}t_0 &= y(\boldsymbol{c}) \\ t_1 &= \textstyle\sum_{j_1}\frac{1}{j_1!}\sum_{i_1=1}^{N}\frac{\partial^{j_1}y}{\partial x_{i_1}^{j_1}}(\boldsymbol{c})(x_{i_1}-c_{i_1})^{j_1} \\ t_2 &= \textstyle\sum_{j_1,j_2}\frac{1}{j_1!j_2!}\sum_{i_1<i_2}\frac{\partial^{j_1+j_2}y}{\partial x_{i_1}^{j_1}\partial x_{i_2}^{j_2}}(\boldsymbol{c})(x_{i_1}-c_{i_1})^{j_1}(x_{i_2}-c_{i_2})^{j_2} \\ &\vdots \\ t_S &= \textstyle\sum_{j_1,\ldots,j_S}\frac{1}{j_1!\ldots j_S!}\sum_{i_1<\cdots<i_S}\frac{\partial^{j_1+\cdots+j_S}y}{\partial x_{i_1}^{j_1}\ldots\partial x_{i_S}^{j_S}}(\boldsymbol{c})(x_{i_1}-c_{i_1})^{j_1}\ldots(x_{i_S}-c_{i_S})^{j_S}\end{aligned} \tag{10}$$

Using Eqs. (9) and (10), it can be shown that $\hat{y}_S(\boldsymbol{x})$ in Eq. (8) consists of all terms of the Taylor series of $y(\boldsymbol{x})$ that have less than or equal to S variables [20]. The expanded form of Eq. (8), when compared with the Taylor expansion of $y(\boldsymbol{x})$, indicates that the residual error in the S-variate approximation is $y(\boldsymbol{x})-\hat{y}_S(\boldsymbol{x})=\mathcal{R}_{S+1}$, where the remainder $\mathcal{R}_{S+1}$ includes terms of dimension $S+1$ and higher. When $S=1$, Eq. (8) degenerates to the univariate approximation (Eq. (4)). When $S=2$, it becomes the bivariate approximation (Eq. (6)). Similarly, trivariate, quadrivariate, and other higher-variate approximations can be derived by appropriately selecting the value of S. In the limit, when $S=N$, Eq. (8) converges to the exact function $y(\boldsymbol{x})$. In other words, the proposed decomposition generates convergent sequence of approximations of $y(\boldsymbol{x})$.

2.4. Remarks

The decomposition of a general multivariate function $y(\boldsymbol{x})$ can be viewed as a finite sum

$$y(\boldsymbol{x})=\underbrace{\underbrace{\underbrace{y_0+\sum_{i=1}^{N}y_i(x_i)}_{=\hat{y}_1(\boldsymbol{x})}+\sum_{\substack{i_1,i_2=1\\ i_1<i_2}}^{N}y_{i_1i_2}(x_{i_1},x_{i_2})}_{=\hat{y}_2(x)}+\cdots+\sum_{\substack{i_1,\ldots,i_S=1\\ i_1<\cdots<i_S}}^{N}y_{i_1\ldots i_S}(x_{i_1},\ldots,x_{i_s})}_{=\hat{y}_S(x)}+\cdots+y_{12\ldots N}(x_1,\ldots,x_N), \tag{11}$$

where y_0 is a constant, $y_i(x_i)$ is a univariate component function representing independent contribution to $y(\boldsymbol{x})$ by

input variable x_i acting alone, $y_{i_1 i_2}(x_{i_1}, x_{i_2})$ is a bivariate component function describing cooperative influence of two input variables x_{i_1} and x_{i_2}, $y_{i_1 \ldots i_S}(x_{i_1}, \ldots, x_{i_S})$ is an S-variate component function quantifying cooperative effects of S input variables $x_{i_1}, \ldots, x_{i_S}$, and so on. By comparing Eqs. (4) and (6) with Eq. (11), the proposed univariate and bivariate approximations provide two- and three-term approximants, respectively, of the finite decomposition. In general, the S-variate approximation in Eq. (8) yields the $S+1$-term approximant of the decomposition. The fundamental conjecture underlying this work is that component functions arising in proposed decomposition will exhibit insignificant S-variate effects cooperatively when $S \to N$, leading to useful lower-variate approximations of a high-dimensional function. Indeed, this is the major motivation of the reliability methods developed.

It is worth noting that the univariate and bivariate approximations should not be viewed as first- or second-order Taylor series expansions nor do they limit the nonlinearity of $y(\boldsymbol{x})$. According to Eqs. (5) and (7), all higher-order univariate and bivariate terms of $y(\boldsymbol{x})$, respectively, are included in the proposed approximations. Furthermore, the approximations contain contributions from all input variables.

3. Response surface generation

Consider the univariate terms $y_i(x_i) \equiv y(c_1, \ldots, c_{i-1}, x_i, c_{i+1}, \ldots, c_N)$ in Eqs. (4) and (6). If for $x_i = x_i^{(j)}$, n function values

$$y_i(x_i^{(j)}) = y(c_1, \ldots, c_{i-1}, x_i^{(j)}, c_{i+1}, \ldots, c_N); \quad j = 1, 2, \ldots, n \tag{12}$$

are given, the function value for arbitrary x_i can be obtained using the Lagrange interpolation as

$$y_i(x_i) = \sum_{j=1}^{n} \phi_j(x_i) y_i(x_i^{(j)}), \tag{13}$$

where the shape function $\phi_j(x_i)$ is defined as

$$\phi_j(x_i) = \frac{(x_i - x_i^{(1)}) \ldots (x_i - x_i^{(j-1)})(x_i - x_i^{(j+1)}) \ldots (x_i - x_i^{(n)})}{(x_i^{(j)} - x_i^{(1)}) \ldots (x_i^{(j)} - x_i^{(j-1)})(x_i^{(j)} - x_i^{(j+1)}) \ldots (x_i^{(j)} - x_i^{(n)})}. \tag{14}$$

By using Eq. (13), arbitrarily many function values of $y_i(x_i)$ can be generated if n function values are given. The same idea can be applied to the bivariate terms $y_{i_1 i_2}(x_{i_1}, x_{i_2}) \equiv y(c_1, \ldots, c_{i_1-1}, x_{i_1}, c_{i_1+1}, \ldots, c_{i_2-1}, x_{i_2}, c_{i_2+1}, \ldots, c_N)$ in Eq. (6). If for $x_{i_1} = x_{i_1}^{(j_1)}$ and $x_{i_2} = x_{i_2}^{(j_2)}$, n^2 function values

$$y_{i_1 i_2}(x_{i_1}^{(j_1)}, x_{i_2}^{(j_2)}) \equiv y(c_1, \ldots, c_{i_1-1}, x_{i_1}^{(j_1)}, c_{i_1+1}, \ldots, c_{i_2-1}, x_{i_2}^{(j_2)}, c_{i_2+1}, \ldots, c_N); \quad j_1 = 1, 2, \ldots, n; \quad j_2 = 1, 2, \ldots, n \tag{15}$$

are given, the function value $y_{i_1 i_2}(x_{i_1}, x_{i_2})$ for arbitrary point (x_{i_1}, x_{i_2}) can be obtained using the Lagrange interpolation as

$$y_{i_1 i_2}(x_{i_1}, x_{i_2}) = \sum_{j_2=1}^{n} \sum_{j_1=1}^{n} \phi_{j_1}(x_{i_1}) \phi_{j_2}(x_{i_2}) y_{i_1 i_2}(x_{i_1}^{(j_1)}, x_{i_2}^{(j_2)}), \tag{16}$$

where shape functions $\phi_{j_1}(x_{i_1})$ and $\phi_{j_2}(x_{i_2})$ are defined in Eq. (14). Note that there are n and n^2 performance function evaluations involved in Eqs. (13) and (16), respectively. Therefore, the total cost for univariate approximation entails a maximum of $nN+1$ function evaluations, and for bivariate approximation, $N(N-1)n^2/2 + nN + 1$ maximum function evaluations are required. More accurate multivariate approximations can be developed in the similar way. However, because of much higher cost, only univariate and bivariate approximations will be examined in this paper.

4. Monte Carlo simulation

4.1. Component reliability analysis

For component reliability analysis, the Monte Carlo estimates $P_{\mathrm{F},1}$ and $P_{\mathrm{F},2}$ of the failure probability employing univariate and bivariate approximations, respectively, are

$$P_{\mathrm{F},1} = \frac{1}{N_S} \sum_{i=1}^{N_S} \mathcal{I}[\hat{y}_1(\boldsymbol{x}^{(i)}) < 0] \tag{17}$$

$$P_{\mathrm{F},2} = \frac{1}{N_S} \sum_{i=1}^{N_S} \mathcal{I}[\hat{y}_2(\boldsymbol{x}^{(i)}) < 0], \tag{18}$$

where $\boldsymbol{x}^{(i)}$ is the ith realization of $\boldsymbol{X}$, N_S is the sample size, and $\mathcal{I}[\cdot]$ is an indicator function such that $\mathcal{I} = 1$ if $\boldsymbol{x}^{(i)}$ is in the failure set (i.e. when $\hat{y}_1(\boldsymbol{x}^{(i)}) < 0$ for univariate approximation and when $\hat{y}_2(\boldsymbol{x}^{(i)}) < 0$ for bivariate approximation of the performance function) and zero otherwise.

4.2. System reliability analysis

For system reliability analysis involving union and intersection of m failure sets, similar decomposition and response surface approximations can be performed for each performance function. Let $\Omega_{\mathrm{F}} = \{\boldsymbol{x} : \cup_{k=1}^{m} y^{(k)}(\boldsymbol{x}) < 0\}$ and $\Omega_{\mathrm{F}} = \{\boldsymbol{x} : \cap_{k=1}^{m} y^{(k)}(\boldsymbol{x}) < 0\}$ denote component failure sets in series and parallel systems, respectively, where $y^{(k)}(\boldsymbol{x})$ is the kth performance function. Hence, the Monte Carlo estimates $P_{\mathrm{F},1}$ and $P_{\mathrm{F},2}$ using univariate and bivariate approximations,

respectively, are

$$P_{\mathrm{F},1} = \begin{cases} \dfrac{1}{N_S}\displaystyle\sum_{i=1}^{N_S} \mathcal{I}\left[\bigcup_{k=1}^{m} \hat{y}_1^{(k)}(\boldsymbol{x}^{(i)}) < 0\right], & \text{series system} \\ \dfrac{1}{N_S}\displaystyle\sum_{i=1}^{N_S} \mathcal{I}\left[\bigcap_{k=1}^{m} \hat{y}_1^{(k)}(\boldsymbol{x}^{(i)}) < 0\right], & \text{parallel system} \end{cases} \tag{19}$$

$$P_{\mathrm{F},2} = \begin{cases} \dfrac{1}{N_S}\displaystyle\sum_{i=1}^{N_S} \mathcal{I}\left[\bigcup_{k=1}^{m} \hat{y}_2^{(k)}(\boldsymbol{x}^{(i)}) < 0\right], & \text{series system} \\ \dfrac{1}{N_S}\displaystyle\sum_{i=1}^{N_S} \mathcal{I}\left[\bigcap_{k=1}^{m} \hat{y}_2^{(k)}(\boldsymbol{x}^{(i)}) < 0\right], & \text{parallel system} \end{cases}, \tag{20}$$

where $\mathcal{I}[\cdot]$ is another indicator function such that $\mathcal{I} = 1$ if $\boldsymbol{x}^{(i)}$ is in the system failure domain and zero otherwise.

The decomposition methods involving univariate and bivariate approximations, are respectively, defined as univariate and bivariate methods in this paper. Since the proposed methods facilitate explicit lower-dimensional approximations of a general multivariate function, the embedded Monte Carlo simulation can be conducted for any sample size. However, the accuracy and efficiency of the failure probability calculations using Eqs. (17)–(20) depend on both the decomposition and response surface approximations. They will be evaluated using several numerical examples in Section 5.

5. Numerical examples

Two sets of numerical examples, one involving explicit mathematical functions (Examples 1 and 2) and the other involving solid-mechanics/structural problems (Examples 3–7), are presented to illustrate the proposed decomposition methods. Whenever possible, comparisons have been made with alternative approximate (FORM/SORM) and several simulation methods to evaluate the accuracy and computational efficiency of the proposed decomposition methods. All numerical results of decomposition methods are based on the expansion at the mean point. For response surface generation, n (=3, 5, 7 or 9) uniformly distributed points $\mu_i-(n-1)\sigma_i/2$, $\mu_i-(n-3)\sigma_i/2,\ldots$, $\mu_i,\ldots$, $\mu_i+(n-3)\sigma_i/2$, $\mu_i+(n-1)\sigma_i/2$ were deployed at x_i-coordinate with mean μ_i and standard deviation σ_i, leading to $(n-1)N+1$ and $(n-1)^2N(N-1)/2+(n-1)N+1$ function evaluations by univariate and bivariate methods, respectively. In all examples, response surface approximations were constructed in the standard Gaussian space.

When comparing computational efforts by various methods, the number of original performance functions evaluations is chosen as the primary metric in this paper. For the direct Monte Carlo simulation, the number of original function evaluations is the same as the sample size. However, in the proposed decomposition methods, they are different, because the Monte Carlo simulation (although with the same sample size as in direct Monte Carlo simulation) embedded in decomposition methods are conducted using their response surface approximations. The difference in CPU times in evaluating an original function and its response surface approximation is significant when a calculation of the original function involves expensive finite-element or mesh-free analysis, as in Examples 4–7. However, the difference becomes trivial when solving problems involving explicit performance functions, as in Examples 1–3. Hence, the computational effort expressed in terms of function evaluations alone should be carefully interpreted for problems involving explicit functions. Nevertheless, the number of function evaluations provides an objective measure of the computational effort for reliability analysis of realistic problems.

5.1. Example Set I—mathematical functions

Example 1. Consider a component reliability problem with a performance function [21]

$$y(\boldsymbol{X}) = -\frac{1}{2\beta}\sum_{i=1}^{5} X_i^2 - X_6 + \beta, \tag{21}$$

where $X_i \mapsto N(0,1)$, $i=1,\ldots,6$ are independent, standard Gaussian random variables and $\beta=4$. The exact value of the failure probability is $P_{\mathrm{F}} = P\left[y(\boldsymbol{X})<0\right] = 1.30\times10^{-3}$ [21]. Recently, Yonezawa et al. [22], who developed a new simulation method with limited sampling region, predicted the failure probability to be 1.28×10^{-3}, involving 10,000 samples, When this problem was solved by the proposed univariate method, a failure probability of $P_{\mathrm{F},1}=1.32\times10^{-3}$ was calculated using only 13 function evaluations ($n=3$, $N=6$). Hence, the univariate method is not only accurate, but also significantly more efficient than some existing simulation methods (e.g. simulation within limited sampling region [22]). Since the univariate method exactly represents the univariate performance function in Eq. (21), there is no need to pursue the bivariate approximation. However, in many cases, bivariate approximation is needed to achieve improved accuracy and will be illustrated in forthcoming examples.

Example 2. Consider a system reliability problem in which the failure region is bounded by the following two performance functions [13,14]

$$y^{(1)}(\boldsymbol{X}) = -X_1 - X_2 - X_3 + 3\sqrt{3}, \qquad y^{(2)}(\boldsymbol{X}) = -X_3 + 3, \tag{22}$$

where $X_i \mapsto N(0,1)$, $i=1$–3 are independent, standard Gaussian random variables. Both series and parallel systems are considered.

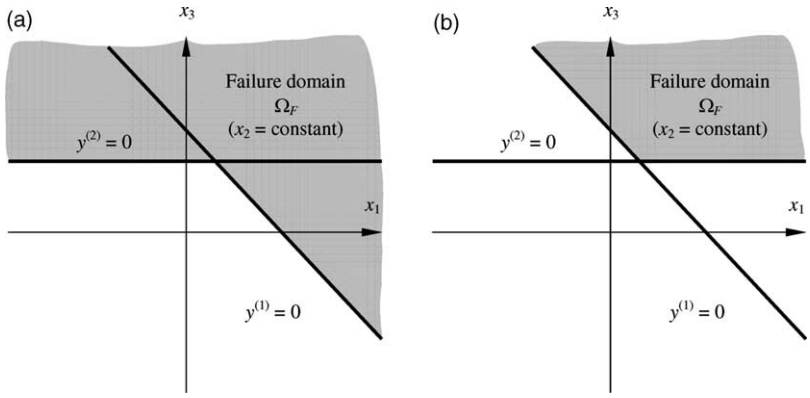

Fig. 1. Failure domain for x_2=constant; (a) series system; (b) parallel system.

Series system

For the series system, the system failure region is defined as $\Omega_F = \{\boldsymbol{x} : y^{(1)}(\boldsymbol{X}) < 0 \cup y^{(2)}(\boldsymbol{X}) < 0\}$, which is sketched in Fig. 1(a) in the $x_1 - x_3$ space when x_2=constant. Katsuki and Frangopol [14] computed Ditlevsen's [3] second-order bounds of the probability of failure to be: $2.53734 \times 10^{-3} \leq P_F \leq 2.61864 \times 10^{-3}$. Table 1 compares the failure probability obtained by the proposed univariate method, second-order bounds, directional simulation using Fekete points by Nie and Ellingwood [13], and the direct Monte Carlo simulation with 10^7 samples. According to Nie and Ellingwood, the directional simulation including Fekete points generates the most accurate and efficient estimation of the failure probability. As can be seen in Table 1, the proposed univariate method provides identical result ($P_{F,1} = 2.585 \times 10^{-3}$) of direct Monte Carlo, but using only 7 (n=3, N=3) function evaluations. This is because both performance functions in Eq. (22) are univariate functions, which are exactly represented by their response surfaces. In contrast, to obtain the same accuracy, the directional simulation involved 36–300 directions; for each direction the radius of the hypersphere segment has to be obtained through numerical methods, which usually takes several function evaluations [13]. Hence, significantly fewer function evaluations are needed in the univariate method.

Table 1
Failure probability for series system

Method	Failure probability ($\times 10^{-3}$)	Number of function evaluations[a]
Univariate method	2.585	7[b]
Second-order bounds[c]	2.537–2.618	
Directional simulation[d]		
Fekete points=36	2.572	
Fekete points=60	2.611	
Fekete points=72	2.570	
Fekete points=96	2.584	
Fekete points=108	2.555	
Fekete points=144	2.580	
Fekete points=240	2.575	
Fekete points=300	2.572	
Direct Monte Carlo simulation	2.585	10,000,000

[a] Total number of times the original performance functions is calculated.
[b] $(3-1)\times 3+1=7$.
[c] See Refs. [3,14].
[d] See Ref. [13]. For each Fekete point, several function evaluations are needed to determine the radius of hypersphere. The total number of function evaluations is not reported.

Parallel system

For the parallel system, the system failure domain is defined as $\Omega_F = \{\boldsymbol{x} : y^{(1)}(\boldsymbol{X}) < 0 \cap y^{(2)}(\boldsymbol{X}) < 0\}$ and is also depicted in Fig. 1(b). The second-order bounds [3] of the probability of failure are: $8.12977 \times 10^{-5} \leq P_F \leq 1.62595 \times 10^{-4}$ [3,13]. The failure probability reported by Katsuki and Frangopol [14] using Hohenbichler's approximation [23] of multinormal integrals is 1.24211×10^{-4}. Nie and Ellingwood [13] also produced various estimations using the directional simulation with Fekete points. Table 2 compares

Table 2
Failure probability for parallel system

Method	Failure probability ($\times 10^{-4}$)	Number of function evaluations[a]
Univariate method	1.303	7[b]
Second-order bounds[c]	0.813–1.626	
Multinormal integrals[d]	1.242	
Directional simulation[e]		
Fekete points=36	1.554	
Fekete points=60	1.235	
Fekete points=72	1.496	
Fekete points=96	1.324	
Fekete points=108	1.475	
Fekete points=144	1.372	
Fekete points=240	1.559	
Fekete points=300	1.526	
Fekete points=1200	1.556	
Direct Monte Carlo simulation	1.303	10,000,000

[a] Total number of times the original performance functions is calculated.
[b] $(3-1)\times 3+1=7$.
[c] See Refs. [3,14].
[d] See Refs. [14,23].
[e] See Ref. [13]. For each Fekete point, several function evaluations are needed to determine the radius of hypersphere. The total number of function evaluations is not reported.

failure probability calculated by the proposed univariate method, second-order bounds, multinormal integrals, Nie and Ellingwood's directional simulation using Fekete points, and direct Monte Carlo simulation with 10^7 samples. For the same reason as in the series system, the probability estimates ($P_{F,1}=1.303\times10^{-4}$) by the univariate method and direct Monte Carlo simulation are identical. According to Table 2, only 7 function evaluations are needed by the univariate method. To achieve the same level of accuracy, the directional simulation required 96 simulating directions. Hence, the proposed univariate method is more efficient than the directional simulation for both series and parallel systems in this example.

5.2. Example Set II—structural and solid-mechanics problems

Example 3. *Rigid-Plastic Portal Frame Structure*. Ditlevsen [24] and Nie and Ellingwood [13] studied the rigid-plastic frame structure of Fig. 2 by the directional simulation method. This structure can be analyzed as a series system of three limit-state functions (collapse mechanisms), which, according to the principle of virtual work, are

$$\begin{aligned} y^{(1)}(\boldsymbol{X}) &= X_2 + 2X_3 + X_4 - Gb \\ y^{(2)}(\boldsymbol{X}) &= X_1 + X_2 + X_4 + X_5 - Fa \\ y^{(3)}(\boldsymbol{X}) &= X_1 + 2X_3 + 2X_4 + X_5 - Fa - Gb, \end{aligned} \tag{23}$$

where $y^{(1)}(\boldsymbol{X})$, $y^{(2)}(\boldsymbol{X})$ and $y^{(3)}(\boldsymbol{X})$ are component limit-state functions for beam, sway and combined mechanisms, respectively. The yield moments X_j, $j=1,\ldots,5$, at hinge points are independent and identically distributed lognormal random variables, with unit mean and 25% coefficient of variation. The lateral force F, vertical force G and distances a and b are constants, with $Gb=1.15$ and $Fa=2.4$. The failure domain is defined as: $\Omega_F=\{\boldsymbol{x}: y^{(1)}(\boldsymbol{X})<0\cup y^{(2)}(\boldsymbol{X})<0\cup y^{(3)}(\boldsymbol{X})<0\}$.

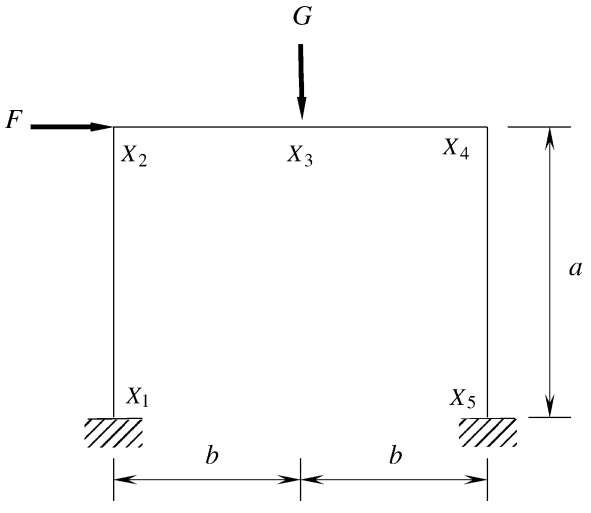

Fig. 2. A portal frame as rigid-plastic system.

Table 3
Failure probability for portal frame

Method	Failure probability ($\times10^{-5}$)	Number of function evaluations[a]
Univariate method	5.544	41[b]
First-order bounds[c]	3.12–5.68	
Second-order bounds[c]	5.200–5.200	
Directional simulation[d]	5.452	
Directional simulation[e]		
Fekete points = 480	5.427	
Fekete points = 604	5.283	
Fekete points = 640	5.382	
Fekete points = 800	5.564	
Fekete points = 960	5.495	
Fekete points = 2080	5.451	
Direct Monte Carlo simulation	5.544	100,000,000

[a] Total number of times the original performance functions is calculated.
[b] $(9-1)\times5+1=41$.
[c] See Refs. [3,13].
[d] A solution by large-scale directional simulation; see Ref. [13].
[e] See Ref. [13]. For each Fekete point, several function evaluations are needed to determine the radius of hypersphere. The total number of function evaluations is not reported.

Table 3 lists the system failure probabilities of the frame, which are calculated by first- and second-order bounds [3,13], a large-scale directional simulation reported in Ref. [13], Nie and Ellingwood's directional simulation involving 480–2080 Fekete points [13], proposed univariate method involving 41 ($n=9$, $N=5$) function evaluations, and direct Monte Carlo simulation involving 10^8 samples. The results in Table 3 indicate that the univariate method provides identical result ($P_{F,1}=5.544\times10^{-5}$) of the direct Monte Carlo simulation. The directional simulations also yield failure probabilities close to the direct Monte Carlo result. But, the proposed method requires very few function evaluations to generate an accurate result.

Example 4. *Ten-Bar Truss Structure (Linear-Elastic)*. A ten-bar, linear-elastic, truss structure, shown in Fig. 3, was studied in this example to examine the accuracy and efficiency of the proposed reliability method. The Young's modulus of the material is 10^7 psi. Two concentrated forces of 10^5 lb are applied at nodes 2 and 3, as shown in Fig. 3. The cross section area X_i, $i=1,\ldots,10$ for each bar is normally distributed random variable with mean $\mu=2.5$ in. and standard deviation $\sigma=0.5$ in. According to the loading condition, the maximum displacement $[(v_3(X_1,\ldots,X_{10}))]$ occurs at node 3, where a permissible displacement is limited to 18 in. Hence, the limit-state function is

$$y(\boldsymbol{X}) = 18 - v_3(X_1,\ldots,X_{10}). \tag{24}$$

Table 4 shows the failure probability of the truss structure, calculated using the proposed univariate method, FORM, three variants of SORM due to Breitung [4], Hohenbeichler [5] and Cai and Elishakoff [6], and direct

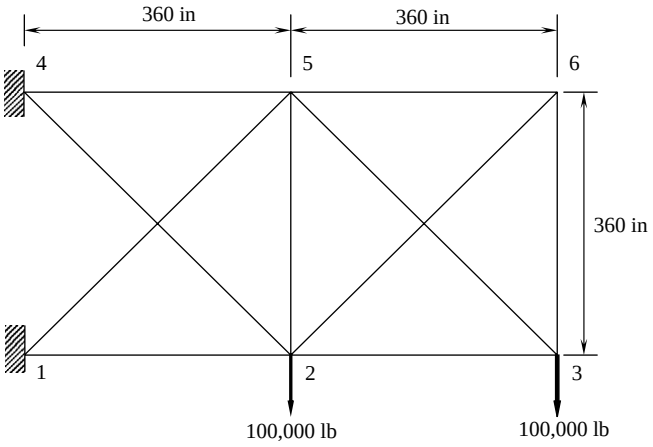

Fig. 3. A ten-bar truss structure with random cross-sectional areas.

Monte Carlo simulation (10^6 samples). For the univariate method, seven uniformly distributed points between $\mu-3\sigma$ and $\mu+3\sigma$ were deployed for function evaluations at each dimension. As can be seen from Table 4, the univariate method predicts the failure probability more accurately than FORM and all three variants of SORM, yet the number of function evaluations is less than FORM and much less than SORM. Furthermore, the proposed method does not require any response derivatives as required by FORM/SORM in finding the MPP.

Example 5. *Stochastic Mesh-Free Analysis of Plate with a Hole (Linear-Elastic)*. Consider a square plate with a centrally located circular hole, as shown in Fig. 4(a). The plate has a dimension of $2L=40$ units, a hole with diameter $2a=2$ units, and is subjected to a uniformly distributed load of magnitude $\sigma^{\infty}=1$ unit. The Poisson's ratio ν was selected to be 0.3. The elastic modulus was assumed to be a homogeneous random field and symmetrically distributed with respect to x_1- and x_2-axes [see Fig. 4(a)]. The modulus of elasticity $E(\boldsymbol{x})$ was represented by a homogeneous, lognormal translation field $E(\boldsymbol{x})=c_{\alpha}\exp[\alpha(\boldsymbol{x})]$, with mean $\mu_E=1$ unit and standard deviation $\sigma_E=0.2$ or 0.5 for which $\alpha(\boldsymbol{x})$ is a *zero*-mean, homogeneous, Gaussian random field

Table 4
Failure probability for ten-bar truss

Method	Failure probability	Number of function evaluations[a]
Univariate method	0.1357	61[b]
FORM	0.0863	127
SORM (Breitung)[c]	0.1286	506
SORM (Hohenbichler)[d]	0.1524	506
SORM (Cai and Elishakoff)[e]	0.1467	506
Direct Monte Carlo simulation	0.1397	1,000,000

[a] Total number of times the original performance functions is calculated.
[b] $(7-1)\times 10+1=61$.
[c] See Ref. [4].
[d] See Ref. [5].
[e] See Ref. [6].

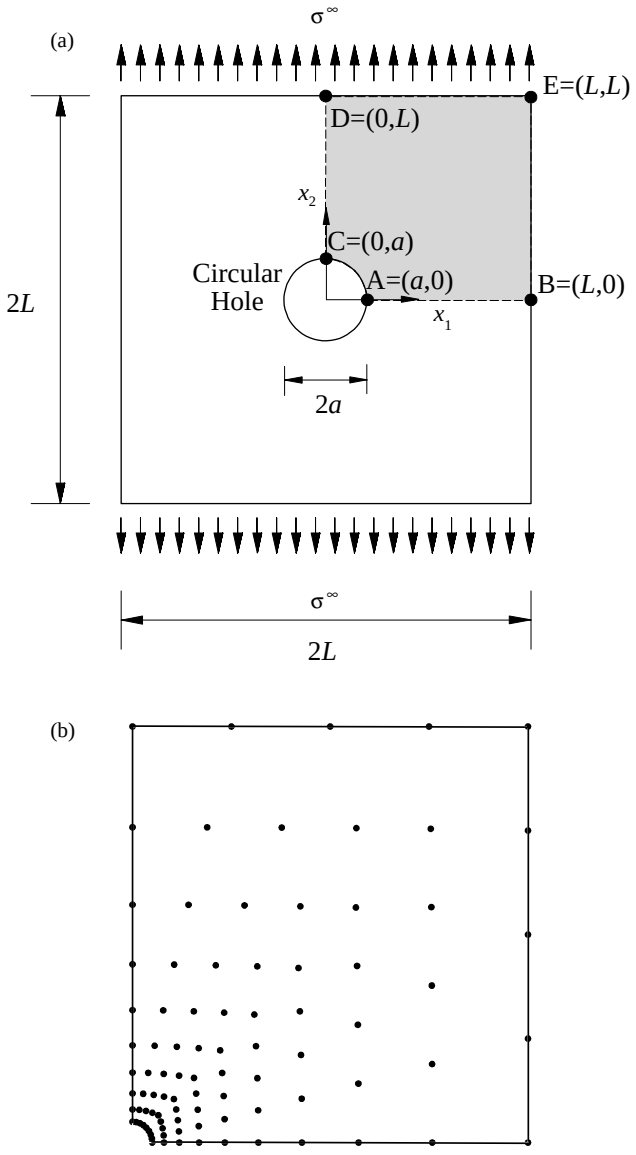

Fig. 4. A square plate with a hole subjected to uniformly distributed tension; (a) geometry and loads; (b) meshless discretization.

with standard deviation $\sigma_{\alpha}=\sqrt{\ln(1+\sigma_E^2/\mu_E^2)}$, an exponential covariance function represented by

$$\Gamma_{\alpha}(\boldsymbol{\xi}) = \mathbb{E}[\alpha(\boldsymbol{x})\alpha(\boldsymbol{x}+\boldsymbol{\xi})] = \sigma_{\alpha}^2\exp\left[-\frac{|\xi_1|+|\xi_2|}{bL}\right], \qquad \forall\,\boldsymbol{x},\ \boldsymbol{x}+\boldsymbol{\xi}\in\mathcal{D}, \quad (25)$$

where $\mathcal{D}\subset\mathbb{R}^2$ is the domain of the random field represented by the shaded area in Fig. 4(a), and

$$c_{\alpha} = \mu_E\exp(-\sigma_{\alpha}^2/2) = \mu_E^2/\sqrt{\mu_E^2+\sigma_E^2}. \quad (26)$$

Due to symmetry, only a quarter of the plate, represented by the region ABEDC and shaded in Fig. 4(a), was

analyzed. Fig. 4(b) presents a meshless discretization of the quarter plate with 90 nodes.

The random field $\alpha(\boldsymbol{x})$ was parameterized using the Karhunen–Loève expansion [25]

$$\alpha(\boldsymbol{x}) \cong \sum_{j=1}^{N} X_j \sqrt{\lambda_j}\phi_j(\boldsymbol{x}). \tag{27}$$

where $X_j \mapsto N(0,1)$, $j=1,\ldots,N$ are standard and independent Gaussian random variables and $\{\lambda_j,\phi_j(\boldsymbol{x})\}$, $j=1,\ldots,N$ are the eigenvalues and eigenfunctions, respectively, of the covariance kernel. Mesh-free shape functions were employed to solve the associated integral equation needed to calculate the eigenvalues and eigenfunctions [26]. Based on the correlation parameter $b=0.5$, a value of $N=8$ was selected to adequately represent $\alpha(\boldsymbol{x})$. Hence, the input uncertainty was represented by an 8-dimensional standard Gaussian vector $\boldsymbol{X} \mapsto N(\boldsymbol{0},\boldsymbol{I})$, where $\boldsymbol{0} \in \mathbb{R}^8$ and $\boldsymbol{I} \in \mathcal{L}(\mathbb{R}^8 \times \mathbb{R}^8)$ are the null vector and identity matrix, respectively.

A stress-based failure criterion at a critical point was employed to calculate the reliability of the plate. If $\sigma_A(X_1,\ldots,X_8)$ denotes the von Mises equivalent stress at point A [see Fig. 4(a)], the limit-state function associated with the von Mises yield criterion is

$$y(\boldsymbol{X}) = S_y - \sigma_A(X_1,\ldots,X_{10}), \tag{28}$$

where S_y is a deterministic yield strength of the material.

Fig. 5(a) and (b) present failure probabilities for various yield strengths, predicted by the proposed decomposition methods, as well as by the direct Monte Carlo simulation (10^5 samples). As can be seen in Fig. 5(a), when the uncertainty of elastic modulus is lower ($\sigma_E=0.2$), both the univariate and bivariate methods provide satisfactory results in comparison with the simulation results. However, when a higher uncertainty is considered ($\sigma_E=0.5$), Fig. 5(b) shows that the accuracy of the failure probability from the bivariate method is slightly higher than that from the univariate method. The number of function evaluations by proposed methods with univariate and bivariate approximations are only 33 and 481, respectively, when $n=5$ and $N=8$. A comparison of total CPU times, shown in Fig. 6, indicates that both decomposition methods are far more efficient than the Monte Carlo simulation. In calculating the CPU times, the overhead cost due to random field discretization, random number generation, and response surface approximations are all included. The overhead cost is comparable to the cost of evaluating the structural response in this particular problem. For this reason, the ratios of CPU times by bivariate and univariate methods and by Monte Carlo and univariate methods, are respectively, only 8 and 1080, as compared with 15 ($\approx$481/33) and 3030 ($\approx$100,000/33), when function evaluations alone are compared. For more complex problems requiring expensive response evaluations, the overhead cost is negligible. In that case, the CPU ratio should approach the ratio of function evaluations. Hence, the proposed methods are effective when a response evaluation entails costly mesh-free or finite-element analysis.

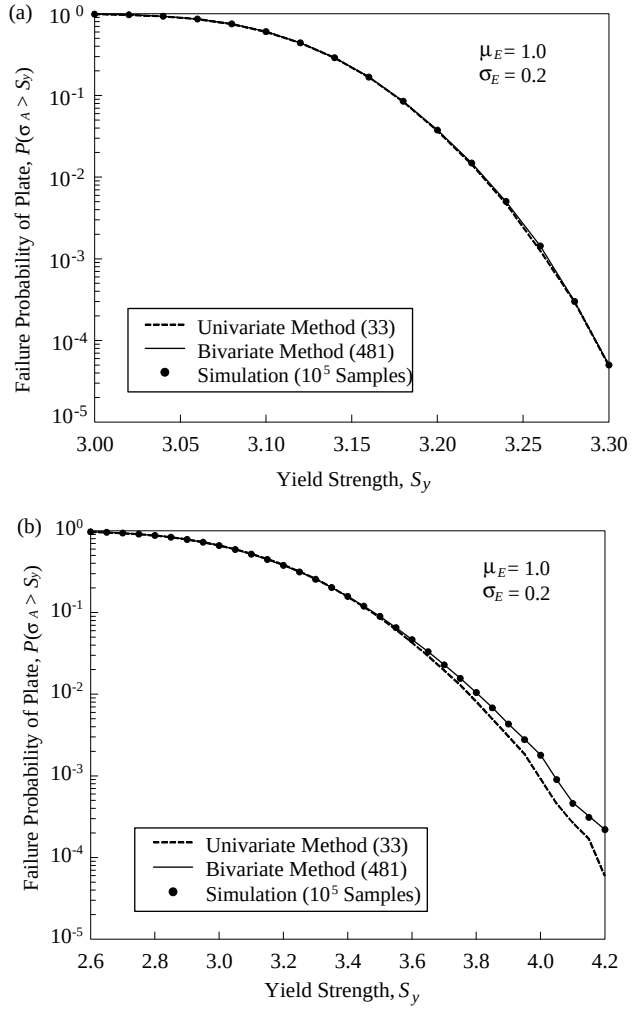

Fig. 5. Failure probability of square plate with a hole; (a) $\sigma_E=0.2$; (b) 0.5.

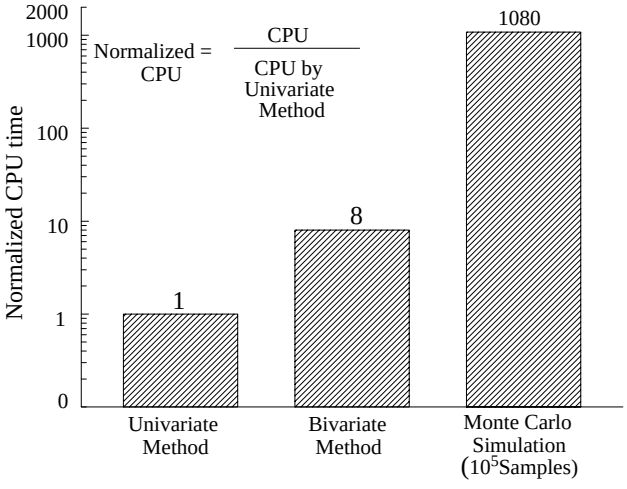

Fig. 6. Comparison of CPU time by various methods.

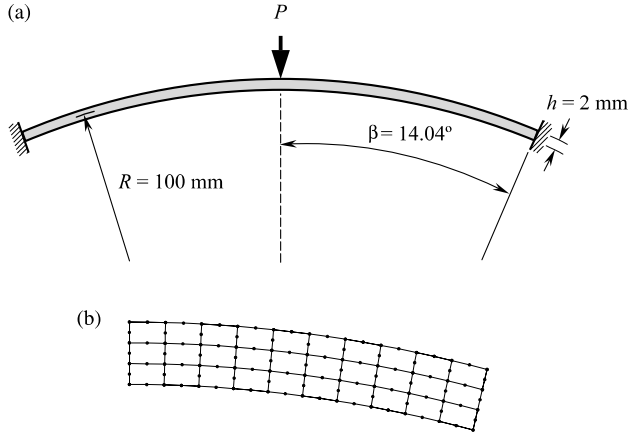

Fig. 7. A shallow arch subject to a concentrated load at midspan; (a) geometry and loads; (b) finite-element discretization.

Example 6. *Stochastic Finite-Element Analysis of Shallow Arch (Nonlinear, Large-Deformation)*. In this example, the proposed decomposition methods were employed to solve a nonlinear problem in solid-mechanics. Fig. 7(a) illustrates a shallow circular arch, with mean radius $R=100$ mm, rectangular cross-section with depth $h=2$ mm, thickness $t=1$ mm, and arc angle $2\beta=28.1°$. The arch, fixed at both ends, was subjected to a concentrated load $P=400$ N at the center. The Poisson's ratio was zero in this example. A finite-element mesh employing 30 8-noded quadrilateral elements was used to model the arch, as shown in Fig. 7(b). The stress analysis involved large-deformation behavior for modeling the geometric nonlinearity of the arch. A plane stress condition was assumed. The modulus of elasticity $E(\boldsymbol{x})$ was represented by a homogeneous, lognormal translation field $E(\boldsymbol{x})=c_\alpha \exp[\alpha(\boldsymbol{x})]$, with mean $\mu_E=80\ \text{kN/mm}^2$ and standard deviation σ_E for which $\alpha(\boldsymbol{x})$ is a zero-mean, homogeneous, Gaussian random field with standard deviation $\sigma_\alpha=\sqrt{\ln(1+\sigma_E^2/\mu_E^2)}$, an exponential covariance function $\Gamma_\alpha(\boldsymbol{\xi})=\mathbb{E}[\alpha(\boldsymbol{x})\alpha(\boldsymbol{x}+\boldsymbol{\xi})]=\sigma_\alpha^2\exp[-||\xi||/(bL)]$, $\forall \boldsymbol{x}$, $\boldsymbol{x}+\boldsymbol{\xi}\in\mathcal{D}$, $b=0.1$; and $c_\alpha=\mu_E\exp(-\sigma_\alpha^2/2)=\mu_E^2/\sqrt{\mu_E^2+\sigma_E^2}$. The Karhunen–Loève expansion was employed to discretize the random field $\alpha(\boldsymbol{x})$ into four standard Gaussian random variables.

Due to uncertainty in the elastic modulus, the deflection u at center point of this arch is stochastic. A displacement-based failure criterion at midspan was employed to calculate the reliability of the plate. If $u(X_1,\ldots,X_4)$ denotes the midspan displacement of the arch, the limit-state function is

$$y(\boldsymbol{X}) = u_0 - u(X_1,\ldots,X_4), \tag{29}$$

where u_0 is a deterministic threshold of displacement.

The proposed univariate and bivariate methods were employed to predict the failure probability of the arch. To evaluate these methods, direct Monte Carlo simulation was performed to generate benchmark solutions. The results, plotted as a function of displacement threshold u_0, are presented in Fig. 8(a) and (b) for two cases of statistical input: (a) $\sigma_E=16$ GPa and (b) $\sigma_E=40$ GPa, representing small and large uncertainties of elastic modulus. The results indicate that the univariate and bivariate methods provide excellent estimates of failure probabilities for both cases of input. For each problem case, the univariate and bivariate methods, respectively, require only 17 and 113 analyses ($n=5$, $N=4$), as opposed to 10^5 analyses in Monte Carlo simulation. Although the accuracy of the univariate method slightly decreases as the uncertainty increases, the bivariate approximation generates very accurate prediction even when the coefficient of variation is 0.5, as indicated by Fig. 8(b).

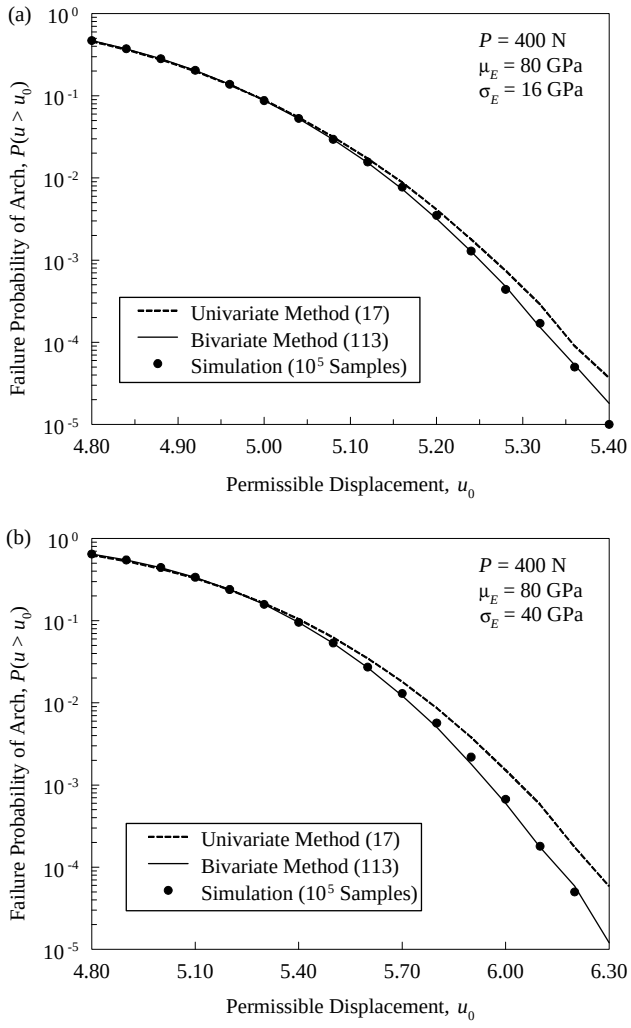

Fig. 8. Failure probability of shallow arch; (a) $\sigma_E=16$ GPa; (b) 40 GPa.

Example 7. *Stochastic Fracture Mechanics (Linear-Elastic)*. The final example involves a nonhomogeneous, functionally graded, edge-cracked plate, presented to illustrate mixed-mode probabilistic fracture-mechanics analysis using the decomposition method. As shown in Fig. 9(a), a functionally graded plate of length $L=16$ units was fixed at the bottom and subjected to a far-field normal

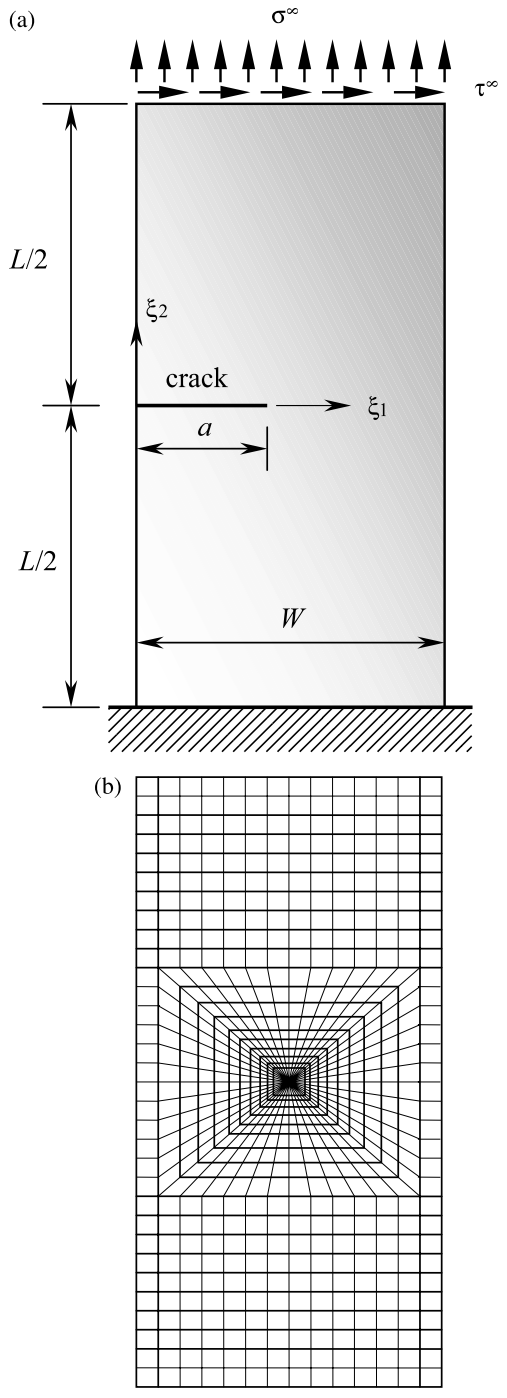

Fig. 9. A functionally graded edge-cracked plate subject to mixed-mode deformation; (a) geometry and loads; (b) finite-element discretization.

stress σ^{∞} and a shear stress τ^{∞} applied at the top. The elastic modulus was assumed to vary smoothly according to a hyperbolic tangent function, given by

$$E(\xi_1,\xi_2)=\frac{E_1+E_2}{2}+\frac{E_1-E_2}{2}\tanh\beta(\xi_1\cos\theta+\xi_2\sin\theta), \tag{30}$$

Table 5
Statistical properties of random input for functionally graded edge-cracked plate

Random variable	Mean	Standard deviation	Probability distribution
a	3.5	0.404	Uniform[a]
W	7.5	0.289	Uniform[b]
σ^{∞}	1	0.1	Gaussian
τ^{∞}	1	0.1	Gaussian
θ	0	0.3	Gaussian
E_1	1	0.1	Lognormal
E_2	3	0.3	Lognormal
β	5	0.5	Lognormal

[a] Uniformly distributed over (2.8,4.2).
[b] Uniformly distributed over (7,8).

where (ξ_1,ξ_2) are spatial coordinates [see Fig. 9(a)], E_1, E_2, β and θ are modulus parameters. The following eight independent random variables were defined: (1) crack length a; (2) plate width W; (3) far-field normal stress σ^{∞}; (4) far-field shear stress τ^{∞}; (5) modulus angle parameter θ; (6) modulus at the left end $E_1=E(0,\xi_2)$; (7) modulus at the right end $E_2=E(W,\xi_2)$; and (8) modulus parameter β. The statistical property of the random input $\boldsymbol{X}=\{a,W,\sigma^{\infty},\tau^{\infty},\theta,E_1,E_2,\beta\}^{\mathrm{T}}$ is defined in Table 5.

Due to far-field stresses the plate is subjected to mixed-mode deformation involving fracture modes I and II [27]. The mixed-mode stress-intensity factors $K_{\mathrm{I}}(\boldsymbol{X})$ and $K_{\mathrm{II}}(\boldsymbol{X})$ were calculated using an interaction integral method [28]. The plate was analyzed using the finite-element method involving a total of 832 8-noded, regular, quadrilateral elements and 48 6-noded, quarter-point (singular), triangular elements at the crack-tip, as shown in Fig. 9(b).

The failure criterion is based on a mixed-mode fracture initiation using the maximum tangential stress theory [27], which leads to the performance function

$$y(\boldsymbol{X})=K_{\mathrm{Ic}}-\left[K_{\mathrm{I}}(\boldsymbol{X})\cos^2\frac{\Theta(\boldsymbol{X})}{2}-\frac{3}{2}K_{\mathrm{II}}(\boldsymbol{X})\sin\Theta(\boldsymbol{X})\right]\times\cos\frac{\Theta(\boldsymbol{X})}{2}, \tag{31}$$

where K_{Ic} is a deterministic fracture toughness, typically measured from small-scale fracture experiments under mode-I and plane strain conditions, and $\Theta_c(\boldsymbol{X})$ is the direction of crack propagation, given by

$$\Theta_c(\boldsymbol{X})=\begin{cases}2\tan^{-1}\left(\dfrac{1-\sqrt{1+8[K_{\mathrm{II}}(\boldsymbol{X})/K_{\mathrm{I}}(\boldsymbol{X})]^2}}{4K_{\mathrm{II}}(\boldsymbol{X})/K_{\mathrm{I}}(\boldsymbol{X})}\right), & \text{if } K_{\mathrm{II}}(\boldsymbol{X})>0\\ 2\tan^{-1}\left(\dfrac{1+\sqrt{1+8[K_{\mathrm{II}}(\boldsymbol{X})/K_{\mathrm{I}}(\boldsymbol{X})]^2}}{4K_{\mathrm{II}}(\boldsymbol{X})/K_{\mathrm{I}}(\boldsymbol{X})}\right), & \text{if } K_{\mathrm{II}}(\boldsymbol{X})<0\end{cases}. \tag{32}$$

The failure probability $P_{\mathrm{F}}=P[y(\boldsymbol{X})<0]$ was predicted using the proposed decomposition methods and compared

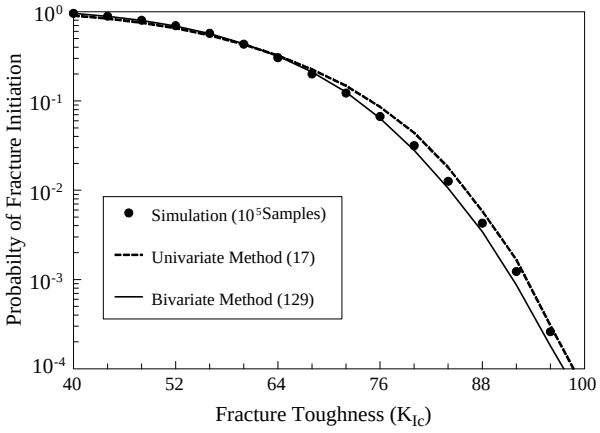

Fig. 10. Probability of fracture initiation in functionally graded edge-cracked plate.

with the direct Monte Carlo simulation, as shown in Fig. 10. In Fig. 10, the failure probability is plotted as a function of fracture toughness K_{Ic}. Using $n=3$ and $N=8$, the univariate and bivariate methods required only 17 and 129 functions evaluations (finite-element analyses), respectively, whereas 10^5 finite-element analyses were performed by the Monte Carlo simulation. The results clearly show that both the univariate and bivariate methods can calculate probability of fracture initiation accurately and efficiently.

6. Conclusions

New computational methods, referred to as decomposition methods, were developed for predicting reliability of structural and mechanical systems subject to random loads, material properties, and geometry. The methods involve a novel function decomposition that facilitates univariate and bivariate approximations of a general multivariate function, response surface generation of univariate and bivariate functions, and Monte Carlo simulation. Due to a small number of original function evaluations, the proposed methods are very effective, particularly when a response evaluation entails costly finite-element, mesh-free, or other numerical analysis. The methods can solve both component and system reliability problems. Seven numerical examples involving elementary mathematical functions and solid-mechanics problems illustrate the proposed method. Results indicate that the methods developed provide accurate and computationally efficient estimates of probability of failure.

Acknowledgements

The authors would like to acknowledge the financial support by the US National Science Foundation under Grant No. DMI-0355487.

References

[1] Madsen HO, Krenk S, Lind NC. Methods of structural safety. Englewood Cliffs, NJ: Prentice-Hall; 1986.
[2] Rackwitz R. Reliability analysis—a review and some perspectives. Struct Saf 2001;23(4):365–95.
[3] Ditlevsen O, Madsen HO. Structural reliability methods. Chichester: Wiley; 1996.
[4] Breitung K. Asymptotic approximations for multinormal integrals. ASCE J Eng Mech 1984;110(3):357–66.
[5] Hohenbichler M, Gollwitzer S, Kruse W, Rackwitz R. New light on first- and second-order reliability methods. Struct Saf 1987;4:267–84.
[6] Cai GQ, Elishakoff I. Refined second-order reliability analysis. Struct Saf 1994;14:267–76.
[7] Tvedt L. Distribution of quadratic forms in normal space—application to structural reliability. ASCE J Eng Mech 1990;116(6):1183–97.
[8] Der Kiureghian A, Dakessian T. Multiple design points in first and second-order reliability. Struct Saf 1998;20(1):37–49.
[9] Rubinstein RY. Simulation and the Monte Carlo method. New York: Wiley; 1981.
[10] Niederreiter H, Spanier J. Monte Carlo and quasi-Monte Carlo methods. Berlin: Springer-Verlag; 2000.
[11] Melchers RE. Importance sampling in structural systems. Struct Saf 1989;6:3–10.
[12] Bjerager P. Probability integration by directional simulation. ASCE J Eng Mech 1988;114(8):1285–302.
[13] Nie J, Ellingwood BR. Directional methods for structural reliability analysis. Struct Saf 2000;22:233–49.
[14] Katsuki S, Frangopol DM. Hyperspace division method for structural reliability. ASCE J Eng Mech 1994;120(11):2405–27.
[15] McKay MD, Conover WJ, Beckman RJ. A comparison of three methods for selecting values of input variables in the analysis of output from a computer code. Technometrics 1979;21(2):239–45.
[16] Gilks WR, Richardson S, Spiegelhalter DJ. Markov chain Monte Carlo in practice. London: Chapman-Hall; 1996.
[17] Au SK, Beck JL. Estimation of small failure probabilities in high dimensions by subset simulation. Probab Eng Mech 2001;16(4):263–77.
[18] Schuëller GI, Pradlwarter HW, Koutsourelakis PS. A critical appraisal of reliability estimation procedures for high dimensions. Probab Eng Mech 2004;19(4):463–74.
[19] Rahman S, Xu H. A univariate dimension-reduction method for multi-dimensional integration in stochastic mechanics. Probab Eng Mech 2004;19(4):393–408.
[20] Xu H, Rahman S. A generalized dimension-reduction method for multi-dimensional integration in stochastic mechanics. Int J Numer Methods Eng 2004;61:1992–2019.
[21] Harbitz A. An efficient sampling method for probability of failure calculation. Struct Saf 1986;3:104–15.
[22] Yonezawa M, Okuda S, Park YT. Structural reliability estimation based on simulation within limited sampling region. Int J Prod Econ 1999;60–61:607–12.
[23] Hohenbichler M, Rackwitz R. Reliability of parallel systems under imposed strain. ASCE J Eng Mech 1983;109(3):896–907.
[24] Ditlevsen O, Melchers RE, Gluver H. General multi-dimensional probability integration by directional simulation. Comput Struct 1990;36(2):355–68.
[25] Davenport WB, Root WL. An introduction to the theory of random signals and noise. New York: McGraw-Hill; 1958.
[26] Rahman S, Xu H. A meshless method for computational stochastic mechanics. Int J Comput Methods Eng Sci Mech 2005;6:41–58.
[27] Anderson TL. Fracture mechanics: fundamentals and applications. 2nd ed. Boca Raton, Florida: CRC Press Inc.; 1995.
[28] Rao BN, Rahman S. Meshfree analysis of cracks in isotropic functionally graded materials. Eng Fract Mech 2003;70(1):1–27.